Electron-Rich Oxoruthenium(IV) Cleavage Agents: A Zero-Order Rate Law for DNA Catalysis

Thomas W. Welch,† Suzanne A. Ciftan, P. S. White, and H. Holden Thorp*

Department of Chemistry, The University of North Carolina, Chapel Hill, North Carolina 27599-3290

Received April 3, 1997[⊗]

A new family of oxoruthenium(IV) complexes based on $[(DAMP)(L)RuO]^{2+}$ have been prepared where DAMP = 2,6-bis((dimethylamino)methyl)pyridine and L = 2,2′-bipyridine (bpy), 1,10-phenanthroline (phen), or dipyridophenazine (dppz). The structures of $[(DAMP)(bpy)RuO]^{2+}$ and $[(DAMP)(phen)RuO]^{2+}$ were determined by X-ray crystallography. The Ru−O bond lengths (1.805(3) and 1.814(4) Å, respectively) are indicative of multiple bonding, as expected for oxoruthenium(IV), and clear steric protection of the Ru═O moiety is provided by the DAMP ligand. Cyclic voltammetry shows that the tertiary amine functionalities of the DAMP ligand stabilize both the $Ru^{IV}O^{2+}$ and $Ru^{III}OH^{2+}$ redox forms relative to other (polypyridyl)oxoruthenium(IV) complexes. As a result, the oxidations of both *sec*-phenylethanol and *trans*-stilbene are ∼100 times slower for $[(DAMP)(bpy)RuO]^{2+}$ than for $[(bpy)_2(py)RuO]^{2+}$. Accordingly, the reaction mechanisms involve oxidation of substrate only by the $Ru^{IV}O^{2+}$ form with no contribution from direct oxidation by the $Ru^{III}OH^{2+}$ intermediate, which greatly simplifies the kinetic analysis. The $Ru^{IV}O^{2+}$ forms are not effective oxidants of the sugar moiety of mononucleotides; however, the base functionality of guanosine 5′-monophosphate is oxidized at detectable rates. In contrast, cleavage of a hairpin oligonucleotide is detected at both guanine and sugar functionalities, indicating that the oligomer promotes sugar oxidation by increasing the local concentration of the metal complex. The $Ru^{III}OH^{2+}$ form of the DAMP complexes is stable in the absence of DNA but is reduced following a zero-order rate law in the presence of calf thymus DNA. Analysis using a model that resembles Michaelis−Menten kinetics indicates that the binding domain on DNA catalyzes the disproportionation of the complex. The model yields a binding constant and a calculated first-order rate constant that are in good agreement with independent measurements.

The ability of DNA to promote chemical reactions has been noted in a number of systems. Diffusive, bimolecular electron transfers between two cationic metal complexes are accelerated by condensation on the DNA polyanion,[1−3] and nondiffusive electron transfer can occur over relatively large distances between covalently or intercalatively bound partners.[4−7] Labeling of GG sites in single stranded oligomers by cationic platinum complexes is promoted by incorporation of the GG site in longer oligomers,[8] and binding of intercalators to platinated DNA sites is also promoted specifically by double-stranded DNA.[9,10] Recognition of binding sites by DNA-binding proteins is believed to occur through facilitated diffusion of the protein.[11] If DNA is a true catalyst, then the time dependence of the reaction should be zero-order,[12] a feature that has not been observed in previous examples of DNA catalysis of which we are aware. We report here on an oxoruthenium(IV) system where the conversion of a $Ru^{III}OH^{2+}$ intermediate to the thermodynamically more stable $Ru^{II}OH_2^{2+}$ state does exhibit a zero-order time dependence in the presence of DNA. This time dependence was masked by efficient DNA oxidation by the $Ru^{III}OH^{2+}$ form in earlier studies of complexes based on $[(tpy)(bpy)RuO]^{2+}$ (bpy = 2,2′-bipyridine; tpy = 2,2′,2″-terpyridine); however, substitution of a tertiary amine ligand for tpy limits the reactivity of the $Ru^{III}OH^{2+}$ form to disproportionation to $Ru^{II}OH_2^{2+}$ and $Ru^{IV}O^{2+}$, which directly oxidizes DNA or itself to yield another equivalent of $Ru^{II}OH_2^{2+}$. In this latter scenario, the kinetics of disproportionation can be monitored directly via the appearance of the strongly colored $Ru^{II}OH_2^{2+}$ form and clearly show a zero-order time dependence that is DNA-catalyzed. Studies of model substrates show that the new complexes are simply less oxidizing than the parent $[(tpy)(bpy)RuO]^{2+}$ complexes and that the tertiary amine ligand has stabilized the higher oxidation states but has not altered the available oxidation pathways. While we demonstrate here the appropriate kinetic behavior, a true catalyst in the enzyme sense would also exhibit transition-state stabilization,[13] but we do not examine that point here.

An advantage of the oxoruthenium(IV) and oxoosmium(IV) systems is that the kinetics of the reduction of the complex that occurs concomitantly with DNA oxidation can be determined in real time from optical spectra.[14−17] Previous kinetics studies of DNA oxidations by complexes of oxoruthenium(IV)[15] and

† Present address: Novalon Pharmaceutical Corp., 214 W. Cameron Ave., Chapel Hill, NC 27516.

⊗ Abstract published in *Advance ACS Abstracts,* September 15, 1997.

(1) Barton, J. K.; Kumar, C. V.; Turro, N. J. *J. Am. Chem. Soc.* **1986**, *108*, 6391−6393.
(2) Orellana, G.; Kirsch-De Mesmaeker, A.; Barton, J. K.; Turro, N. J. *Photochem. Photobiol.* **1991**, *54*, 499−509.
(3) Fromherz, P.; Rieger, B. *J. Am. Chem. Soc.* **1986**, *108*, 5361−5362.
(4) Meade, T. J.; Kayyem, J. F. *Angew. Chem., Int Ed. Engl.* **1995**, *34*, 352−354.
(5) Murphy, C. J.; Arkin, M. R.; Jenkins, Y.; Ghatlia, N. D.; Bossmann, S. H.; Turro, N. J.; Barton, J. K. *Science* **1993**, *262*, 1025−1029.
(6) Murphy, C. J.; Arkin, M. R.; Ghatalia, N. D.; Bossman, S.; Turro, N. J.; Barton, J. K. *Proc. Natl. Acad. Sci. U.S.A.* **1994**, *91*, 5315−5319.
(7) Arkin, M. R.; Stemp, E. D. A.; Holmlin, R. E.; Barton, J. K.; Hörmann, A.; Olson, E. J. C.; Barbara, P. F. *Science* **1996**, *273*, 475−480.
(8) Elmroth, S. K. C.; Lippard, S. J. *J. Am. Chem. Soc.* **1994**, *117*, 3633−3634.
(9) Ren, T.; Bancroft, D. P.; Sundquist, W. I.; Masschelein, A.; Keck, M. V.; Lippard, S. J. *J. Am. Chem. Soc.* **1993**, *115*, 11341−11352.
(10) Boudvillain, M.; Dalbies, R.; Leng, M. *Met. Ions Biol. Syst.* **1996**, *33*, 87−104.
(11) von Hippel, P. H.; Berg, O. G. *J. Biol. Chem.* **1989**, *264*, 675−678.
(12) Fersht, A. *Enzyme Structure and Mechanism*, 2nd ed.; W. H. Freeman: New York, 1985.
(13) Cech, T. R. *Science* **1987**, *236*, 1532.
(14) Neyhart, G. A.; Cheng, C.-C.; Thorp, H. H. *J. Am. Chem. Soc.* **1995**, *117*, 1463−1471.

S0020-1669(97)00394-7 CCC: $14.00

Scheme 1

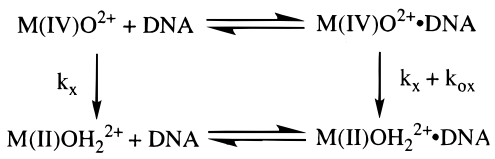

oxoosmium(IV)[16] have shown these reactions to conform partially to the model in Scheme 1, where k_x is the rate of self-inactivation, k_{ox} is the rate of DNA damage, and M = Os, Ru. The high-valent form is pregenerated either chemically or electrochemically from the corresponding M(II) aqua complex and, in the presence of nucleic acid, partitions between bound and free forms according to a characteristic binding constant.[18−20] The synthetic versatility of the group 8 metals allows construction of complexes of the general formula $[(tpy)(L)MOH_2]^{2+}$ where L is bpy, 1,10-phenanthroline (phen), or dipyridophenazine (dppz).[21−23] This set of bidentate aromatic ligands influences the binding affinities for the complexes but retains similar redox potentials for the $M(II)OH_2^{2+}/M(IV)O^{2+}$ couple. The simplicity of Scheme 1 is not realized in these reactions because of comproportionation according to the following:

$$Ru^{IV}O^{2+} + Ru^{II}OH_2^{2+} \rightleftharpoons 2Ru^{III}OH^{2+} \qquad (1)$$

In the case of the tpy complexes, the $Ru^{III}OH^{2+}$ form is a competent oxidant of DNA itself, which significantly complicates the kinetic analysis.

We report here preparations of the oxidants $[(DAMP)(L)RuO]^{2+}$, where L is bpy, phen, and dppz (DAMP = 2,6-bis((dimethylamino)methyl)pyridine). Electronic structure and crystallography data confirm that the RuO group is both electron-rich and sterically protected compared to the tpy analogues. These factors result in slower kinetics and more demanding activation parameters for the $Ru^{IV}O^{2+}$ forms as determined in oxidations of small molecules, and the activation of substrate by the $Ru^{III}OH^{2+}$ form is no longer competitive with disproportionation. Therefore, the $Ru^{III}OH^{2+}$ form can oxidize substrate only via the $Ru^{IV}O^{2+}$ state that is generated by unfavorable disproportionation according to the reverse of eq 1. We show here that DNA oxidation by $[(DAMP)(bpy)Ru^{III}OH]^{2+}$ is catalyzed by DNA with a zero-order time dependence for the appearance of the $[(DAMP)(bpy)Ru^{II}OH_2]^{2+}$ product.

Experimental Section

Materials and Syntheses. Ligands and ligand starting materials were purchased from Aldrich. Dipyridophenazine was synthesized according to published procedures. $RuCl_3 \cdot xH_2O$ was purchased from Johnson-Matthey Aesar. $(DMSO)_4RuCl_2$ was synthesized according to published procedures.[24] Complete preparations of the DAMP complexes are given in the Supporting Information. *sec*-Phenylethanol was purchased from Lancaster. Solvents were purchased from Fisher. Calf thymus DNA and nucleotides were purchased from Sigma. The hairpin oligonucleotide was prepared by automated synthesis in the UNC Department of Pathology. Procedures for the hairpin cleavage reaction and electrophoresis are given in the Supporting Information.

Instrumentation. Optical spectra were obtained using a Hewlett-Packard HP8452 diode array spectrophotometer. Kinetics experiments were carried out using the diode array spectrophotometer thermostatted to 25 °C except for determinations of activation energies, where the circulating water bath was used to vary the temperature over the indicated range. All kinetics experiments were conducted using the perchlorate salts of the metal complexes in 50 mM phosphate buffer unless otherwise noted. Electrochemical measurements were performed in a cell that has been described previously.[25] The working electrode was edge-oriented pyrolytic graphite in cyclic voltammetry experiments. Bulk electrolysis was performed in a three-compartment cell using a reticulated vitreous carbon working electrode. The potential was applied using a platinum wire auxiliary electrode and a Cypress Systems Ag/AgCl electrode as a reference. Voltammograms were collected using an EG&G Princeton Applied Research 273A potentiostat.

DNA Binding Constants. Binding constants for $[(tpy)(L)RuOH_2]^{2+}$ and $[(DAMP)(L)RuOH_2]^{2+}$ where L was bpy or phen were determined by an electrochemical method that uses normal pulse voltammetry to determine the effective diffusion coefficient during DNA titration and quantifies binding based on comparisions to the known diffusion coefficients of free and bound complexes.[26] The binding constant of $[(DAMP)(dppz)RuOH_2]^{2+}$ was determined via absorption titration as previously described.[25]

pK_a Determination. Metal complex salts were dissolved to a concentration of 100 μM in ∼50 mL of distilled water. The pH was raised in $\sim^1/_2$ pH unit increments by adding small amounts of 0.1, 1.0, or 10.0 M NaOH with magnetic stirring. One milliliter of solution was withdrawn after each addition, the UV−visible absorption spectrum was taken, and the aliquot was returned to the original container. The pK_a was determined from a plot of absorbance at the λ_{max} of the $Ru^{III}OH^{2+}$ complex.

X-ray Crystallography. Diffraction-quality crystals of $[(DAMP)(bpy)RuO](ClO_4)_2$ and $[(DAMP)(phen)RuO](ClO_4)_2$ were grown by diffusion of diethyl ether into concentrated acetonitrile solutions of the respective salts at 4 °C. X-ray intensity data were obtained on a Rigaku diffractometer at −130 °C. Data for the bpy complex was collected using the $\theta-2\theta$ scan mode. Cell dimensions were obtained from 42 reflections with 2θ values between 30 and 40°. One of the perchlorate groups was disordered and modeled as two superimposed tetrahedra of isotropic oxygens. Data for the phen complex was collected using the ω scan mode. Cell dimensions were determined from 27 reflections with 2θ values between 30 and 40°. Hydrogen atoms for both complexes were placed in calculated positions in the final refinement using a riding model.

Oxidation of Organic Molecules. Time-resolved visible spectra of reaction solutions were aquired on a Hewlett-Packard HP 8452 diode array spectrophotometer. Aliquots of oxoruthenium(IV) were added to substrate solutions in a 3 mL stoppered cuvette and mixed by hand. The temperature was controlled using a Fisher Isotemp Model 910 circulating ethylene glycol bath. Yields of acetophenone from *sec*-phenylethanol oxidation were determined by extraction into pentane followed by quantitation by UV absorbance at 238 nm where ϵ_{238} = 13 000 M^{-1} cm^{-1}.

Fitting of Spectral−Kinetic Data. The time-resolved spectra taken during oxidations of organic molecules and DNA were processed using the program SPECFIT, whose algorithms are based on the work of Zuberbühler et al.[27] The application of SPECFIT to the kinetics of

(15) Neyhart, G. A.; Grover, N.; Smith, S. R.; Kalsbeck, W. A.; Fairley, T. A.; Cory, M.; Thorp, H. H. *J. Am. Chem. Soc.* **1993**, *115*, 4423.
(16) Cheng, C.-C.; Goll, J. G.; Neyhart, G. A.; Welch, T. W.; Singh, P.; Thorp, H. H. *J. Am. Chem. Soc.* **1995**, *117*, 2970−2980.
(17) Goll, J. G.; Thorp, H. H. *Inorg. Chim. Acta* **1996**, *242*, 219−223.
(18) Satyanarayana, S.; Dabrowiak, J. C.; Chaires, J. B. *Biochemistry* **1992**, *31*, 9319.
(19) Kalsbeck, W. A.; Thorp, H. H. *J. Am. Chem. Soc.* **1993**, *115*, 7146−7151.
(20) Carter, M. T.; Rodriguez, M.; Bard, A. J. *J. Am. Chem. Soc.* **1989**, *111*, 8901.
(21) Gupta, N.; Grover, N.; Neyhart, G. A.; Singh, P.; Thorp, H. H. *Inorg. Chem.* **1993**, *32*, 310.
(22) Gupta, N.; Grover, N.; Neyhart, G. A.; Liang, W.; Singh, P.; Thorp, H. H. *Angew. Chem., Int. Ed. Engl.* **1992**, *31*, 1048.
(23) Takeuchi, K. J.; Thompson, M. S.; Pipes, D. W.; Meyer, T. J. *Inorg. Chem.* **1984**, *23*, 1845.
(24) Evans, I. P.; Spencer, A.; Wilkinson, G. *J. Chem. Soc., Dalton Trans.* **1973**, 204.
(25) Welch, T. W.; Corbett, A. H.; Thorp, H. H. *J. Phys. Chem.* **1995**, *99*, 11757−11763.
(26) Welch, T. W.; Thorp, H. H. *J. Phys. Chem.* **1996**, *100*, 13829−13836.
(27) Maeder, M.; Zuberbühler, A. D. *Anal. Chem.* **1990**, *62*, 2220.

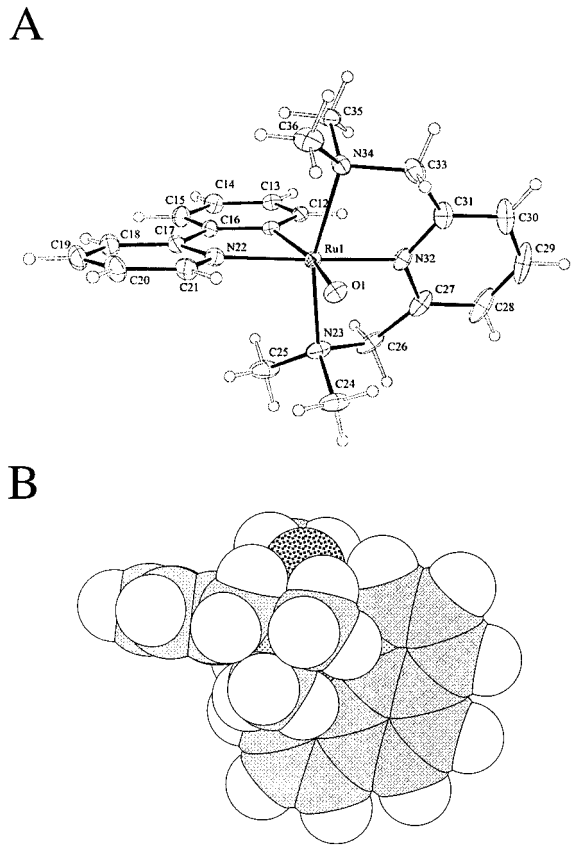

Figure 1. (A) ORTEP representation of the cation in [(DAMP)(bpy)-RuO]$(ClO_4)_2$. Thermal ellipsoids are drawn at 50% probability. Hydrogen atoms are in calculated positions. (B) Space-filling representation of the cation in [(DAMP)(phen)RuO]$(ClO_4)_2$. Non-hydrogen atoms are in positions from the X-ray structure. Hydrogen atoms are in calculated positions.

oxoruthenium(IV) oxidations has been described in detail elsewhere.[28] For the kinetic analyses described here, the time-resolved spectra were subjected to singular value decomposition, and the significant eigenvectors were selected. A mechanism was input into the program, which generated the appropriate set of differential rate equations. After fitting of the rate equations to the spectral data, the output spectra of the colored species were then compared with known spectra that could be obtained independently. In all of the cases described here, all of the output spectra corresponded to one of the three oxidation states $[(DAMP)(bpy)Ru^{IV}O]^{2+}$, $[(DAMP)(bpy)Ru^{III}OH]^{2+}$, and $[(DAMP)(bpy)Ru^{II}OH_2]^{2+}$.

Results

Structure and Properties. The crystal structures of two of the oxoruthenium(IV) forms are presented in an ORTEP represention of $[(DAMP)(bpy)RuO]^{2+}$ and a space-filling representation of $[(DAMP)(phen)RuO]^{2+}$ in Figure 1. The crystal data for both structures and the atomic fractional coordinates are given in the Supporting Information. Selected bond distances and angles are given in Table 1. The ruthenium−oxygen bond lengths of 1.805(3) and 1.814(4) Å for the bpy and phen complexes, respectively, are comparable to the value 1.815(6) Å reported for $[(Me_3TACN)(L)RuO]^{2+}$.[29] When compared to the average Ru−O distance in several $[(tpy)(L)RuOH_2]^{2+}$ complexes of 2.14 Å,[22,30,31] these lengths reflect a higher metal−oxygen bond order. The tertiary amino groups

Table 1. Selected Bond Distances and Bond Angles for $[(DAMP)(bpy)RuO](ClO_4)_2$ and $[(DAMP)(phen)RuO](ClO_4)_2$

	$[(DAMP)(bpy)RuO]^{2+}$	$[(DAMP)(phen)RuO]^{2+}$
Selected Distances (Å)		
Ru(1)−O(1)	1.805(3)	1.814(4)
Ru(1)−N(11)	2.164(3)	2.177(5)
Ru(1)−N(22)	2.088(3)	2.095(5)
Ru(1)−N(23)	2.177(3)	2.170(5)
Ru(1)−N(32)	1.991(3)	1.990(5)
Ru(1)−N(34)	2.151(3)	2.145(5)
Selected Angles (deg)		
O(1)−Ru(1)−N(11)	168.94(12)	168.81(19)
O(1)−Ru(1)−N(22)	92.62(13)	90.76(20)
O(1)−Ru(1)−N(23)	92.58(13)	93.26(19)
O(1)−Ru(1)−N(32)	91.79(13)	92.15(21)
O(1)−Ru(1)−N(34)	87.99(13)	88.42(20)
N(11)−Ru(1)−N(22)	76.52(12)	78.06(18)
N(11)−Ru(1)−N(23)	87.40(12)	88.85(17)
N(11)−Ru(1)−N(32)	99.09(13)	99.03(19)
N(11)−Ru(1)−N(34)	95.70(12)	93.38(18)
N(22)−Ru(1)−N(23)	100.21(14)	101.10(19)
N(22)−Ru(1)−N(32)	175.57(12)	176.84(20)
N(22)−Ru(1)−N(34)	99.21(13)	98.95(20)
N(23)−Ru(1)−N(32)	79.99(14)	79.96(20)
N(23)−Ru(1)−N(34)	160.53(13)	159.86(19)
N(32)−Ru(1)−N(34)	80.53(13)	79.92(20)

are disposed at an angle of ∼169° compared to the trans-tpy nitrogens at 159° in $[(tpy)(bpy)RuOH_2]^{2+}$ [30] and, in the solid state, exhibit a slight twist that is not apparent in the solution NMR. The space-filling model of $[(DAMP)(phen)RuO]^{2+}$ in Figure 1B shows the view along the axis established by the tertiary amines and reveals the oxo group to be sterically protected in three of the four directions perpendicular to the oxometal axis.

The cyclic voltammetry of a 100 μM solution of $[(DAMP)(bpy)RuOH_2]^{2+}$ is presented in Figure 2. Only using an edge-oriented pyrolytic graphite working electrode at a scan rate of 2 mV s^{-1} was it possible to observe two waves over a broad range of pH values. The two waves represent the sequential proton-coupled oxidations of the aquaruthenium(II) complex to the oxoruthenium(IV) form via eqs 1 and 2 at 0.34 and 0.48 V

$$[(DAMP)(bpy)RuOH_2]^{2+} \rightarrow [(DAMP)(bpy)RuOH]^{2+} + H^+ + e^- \quad (2)$$

$$[(DAMP)(bpy)RuOH]^{2+} \rightarrow [(DAMP)(bpy)RuO]^{2+} + H^+ + e^- \quad (3)$$

vs Ag/AgCl, respectively. The Pourbaix diagram, also presented in Figure 2, shows the 60 mV per pH unit dependence typical of proton-coupled electron transfer[21,23,32] with loss of this effect for the (III/II) couple above pH 11.5, the pK_a af the aquaruthenium(II) complex. The complexes $[(DAMP)(bpy)RuOH]^{2+}$ and $[(DAMP)(bpy)RuO]^{2+}$ can be prepared in aqueous buffer from the aqua complex via bulk electrolysis at 0.4 and 0.8 V versus Ag/AgCl, respectively. Figure 3 shows the UV−visible absorption of a 100 μM solution of $[(DAMP)(bpy)RuOH_2]^{2+}$ and the spectra after exhaustive electrolysis at 0.4 and 0.8 V, which generates the Ru(III) and Ru(IV) states, respectively. The extinction coefficients and absorption maxima (λ_{max}) are listed in the Supporting Information and are vitally important in the kinetic analysis.

(28) Stultz, L. K.; Binstead, R. A.; Reynolds, M. S.; Meyer, T. J. *J. Am. Chem. Soc.* **1995**, *117*, 2520−2532.
(29) Cheng, W.-C.; Yu, W.-Y.; Cheung, K.-K.; Che, C.-M. *J. Chem. Soc., Dalton Trans.* **1994**, 57−62.
(30) Seok, W. K. Thesis, University of North Carolina at Chapel Hill, 1988.
(31) Grover, N.; Gupta, N.; Singh, P.; Thorp, H. H. *Inorg. Chem.* **1992**, *31*, 2014.
(32) Moyer, B. A.; Meyer, T. J. *Inorg. Chem.* **1981**, *20*, 436.

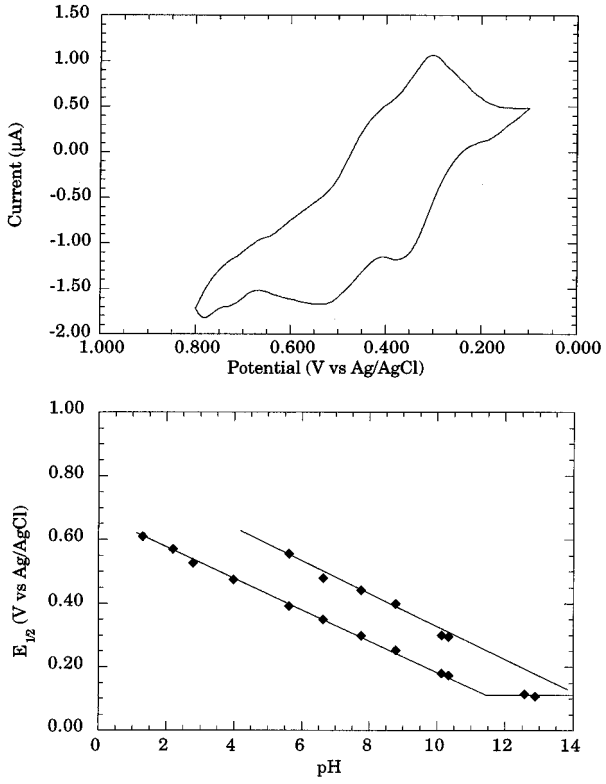

Figure 2. Cyclic voltammetry of a 100 μM solution of [(DAMP)(bpy)$RuOH_2$]$^{2+}$ in 50 mM pH 7 phosphate buffer (top) and Pourbaix Diagram (bottom). Conditions: EOPG working electrode, Pt auxiliary, Ag/AgCl reference, 2 mV s^{-1} scan rate, scanned positively from an initial potential of 0 V.

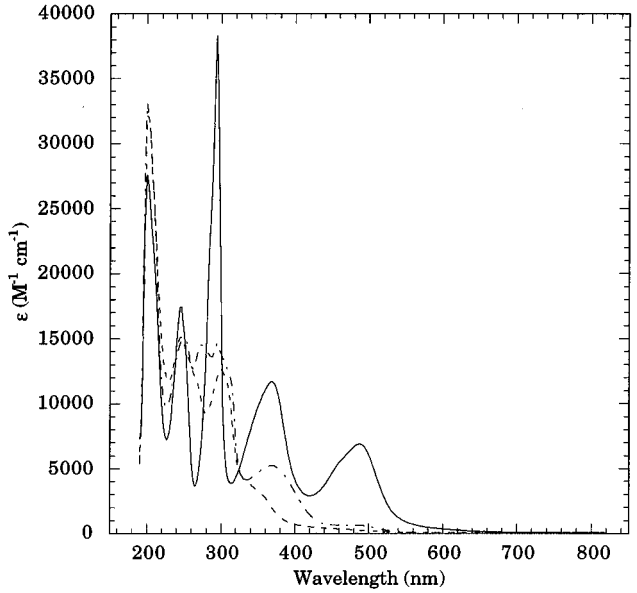

Figure 3. UV−visible spectra of 100 μM solutions of [(DAMP)(bpy)$RuOH_2$]$^{2+}$ (s*M*), (DAMP)(bpy)RuOH]$^{2+}$ (- −), and (DAMP)(bpy)RuO]$^{2+}$ (- - -).

The electronic properties of the DAMP complexes are summarized in Table 2 along with those of the tpy analogues. Given the similarity in pK_a's for the three bidentate ligand types, [(DAMP)(dppz)RuO]$^{2+}$ probably shares the same thermodynamic oxidizing potential as the bpy and phen complexes. Substitution of DAMP for tpy in bpy and phen complexes consistently results in a decrease in the oxidation potentials of approximately 140 mV that must be attributed to the ability of DAMP to provide stronger σ coordination to the metal while eliminating π back-bonding along one axis perpendicular to the oxometal bond. This shift in $E_{1/2}$ is consistent with a change in driving force of a proton-coupled electron transfer equal to ~3.0 kcal mol^{-1}. Thus, from a thermodynamic standpoint, [(tpy)(bpy)RuOH]$^{2+}$ and [(DAMP)(bpy)RuO]$^{2+}$ should be comparable hydrogen atom abstraction agents.

Table 2. Electronic Structure and DNA Binding Properties of DAMP Complexes

complex	*E* (V vs Ag/AgCl) *E*(II/III)	*E*(III/IV)	pK_a	MLCT λ_{max} (nm)	K_b (M^{-1})
[(DAMP)(bpy)$RuOH_2$]$^{2+}$	0.34	0.48	11.5	512	920[a]
[(DAMP)(phen)$RuOH_2$]$^{2+}$	0.39	0.49	11.1	480	1 450[a]
[(DAMP)(dppz)$RuOH_2$]$^{2+}$	0.33[b]		10.7	476	930 000[c]
[(tpy)(bpy)$RuOH_2$]$^{2+}$	0.49	0.62	9.7	508	900[d]
[(tpy)(phen)$RuOH_2$]$^{2+}$	0.48	0.58	10.2	510	1 600[d]
[(tpy)(dppz)$RuOH_2$]$^{2+}$	0.59[b]		8.6		730 000[e]

[a] Determined by electrochemical titration as described in reference 26. [b] Only one wave was resolved; the indicated potential is probably that of the II/III couple. [c] Determined by absorption titration as described in ref 25. [d] Reference 26. [e] Reference 19.

The DNA binding constants (K_b, eq 4) for the aquaruthenium(II) forms of the DAMP complexes were determined by

$$Ru^{II}OH_2^{2+} + DNA \overset{K_b}{\rightleftharpoons} Ru^{II}OH_2^{2+}\cdot DNA \qquad (4)$$

established methods[26] and are given along with those for the tpy complexes in Table 2. As observed with the tpy family, the binding affinity of the complexes increases in the order bpy < phen ≪ dppz. The affinity of the complexes is important for understanding how an increase in the effective concentration due to condensation on the DNA helix influences the reduction kinetics. We have shown previously that the affinities of the similarly charged $Ru^{II}OH_2^{2+}$, $Ru^{III}OH^{2+}$, and $Ru^{IV}O^{2+}$ forms are indistinguishable,[15] a point that will be important in the kinetic analysis described below.

***sec*-Phenylethanol and *trans*-Stilbene Oxidation.** Prior to studies of DNA oxidation, it is useful to determine the mechanisms of oxidation of small molecules where larger concentrations of reactive sites can be achieved and where the available redox pathways and their relative rates can be readily assessed. In particular, we wanted to determine whether both $Ru^{IV}O^{2+}$ and $Ru^{III}OH^{2+}$ were competent oxidants of model substrates and whether stabilization of the higher oxidation states, which is apparent in the electrochemistry, simplifies the kinetics of reduction. Because the 1′ position of deoxyribose is adjacent to the aromatic base, *sec*-phenylethanol has been chosen as a model substrate in aqueous solution, as the weak C−H bond is benzylic.[33] Initial oxidation of guanine is very efficient and is thought to involve more direct oxygen atom transfer;[14] we have therefore examined oxo transfer to *trans*-stilbene in acetonitrile as a model for this reaction. Both oxidations are very efficient with [$(bpy)_2$(py)RuO]$^{2+}$.[28] These model reactions allow comparison of the reactivity of the various RuO complexes; the rate constants for [(tpy)(bpy)RuO]$^{2+}$ fall in the order GMP > phenylethanol > *trans*-stilbene (the rates for [(tpy)(bpy)RuO]$^{2+}$ and [$(bpy)_2$(py)RuO]$^{2+}$ are similar). Determining whether the rate constants for [(DAMP)(bpy)RuO]$^{2+}$ fall in the same order provides a useful test of whether the DAMP ligand simply lowers the overall reactivity or changes the available redox pathways in terms of the accessible multiple-electron redox couples.[34]

Figure 4 shows the spectral changes observed during the reaction of 100 μM [(DAMP)(bpy)RuO]$^{2+}$ with 100 mM *sec*-

(33) Kalsbeck, W. A.; Gingell, D. M.; Malinsky, J. E.; Thorp, H. H. *Inorg. Chem.* **1994**, *33*, 3313−3316.
(34) Meyer, T. J. *J. Electrochem. Soc.* **1984**, *131*, 221C.

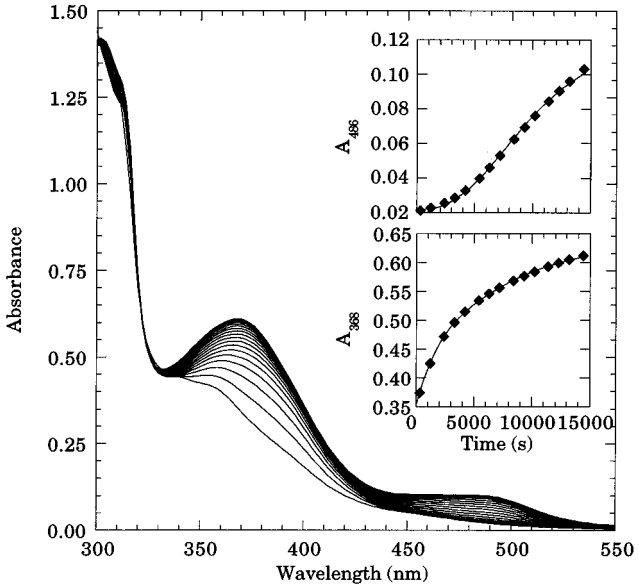

Figure 4. UV−visible spectral changes at 1200 s intervals during the reaction of 100 μM [(DAMP)(bpy)RuO]$^{2+}$ with 100 mM phenylethanol in 50 mM phosphate buffer at pH 7. Inset: Absorbance vs time traces at 368 and 486 nm (symbols) and predicted changes from the fit to the global model described in the text.

phenylethanol over the course of 4 h. The changes consist of a prompt return of absorption at 368 nm followed by a partial recovery of the Ru(II) MLCT band at 486 nm. The inset plots of absorbance versus time reveal a sigmoidal appearance of $Ru^{II}OH_2^{2+}$, and the absorbance at 368 therefore contains kinetic information for both the $Ru^{III}OH^{2+}$ LMCT and high-energy $Ru^{II}OH_2^{2+}$ MLCT bands. Because the isosbestic points for the three complexes are all close to 340 nm, it was not possible to determine separately the kinetics for interconversion of any two of the three available redox forms from single-wavelength plots, as has been done previously for [(tpy)(bpy)RuO]$^{2+}$;[35,36] therefore, all rate constants were determined from singular value decomposition of the complete time-dependent spectra. Only in the case of *sec*-phenylethanol was a complex mechanism (eqs 5 and 6) required to fit the data; all other cases were fit to the conversion of a single reactant to a single product by either a first-order or zero-order process.

The time-dependent spectra for the oxidation of *sec*-phenylethanol were subjected to singular value decomposition, which returned three sets of significant spectral and evolutionary eigenvectors corresponding to three colored species linked by two kinetic processes. In all of the cases described here, the psuedo-first-order reactions were fit to a simple first-order A → B model, and the second-order rate constants were then determined from plots of k_{obs} versus substrate concentration. An alternative method would have been to input the substrate concentrations and have SPECFIT determine second-order rate constants directly; this approach has been used in other cases, mostly where more complicated mechanisms are operative.[28,37] In the case of *sec*-phenylethanol, Marquardt minimization was performed to fit the data to the following model:

$$Ru^{IV}O^{2+} \xrightarrow{k_{1,obs}} Ru^{II}OH_2{}^{2+} \qquad (5)$$

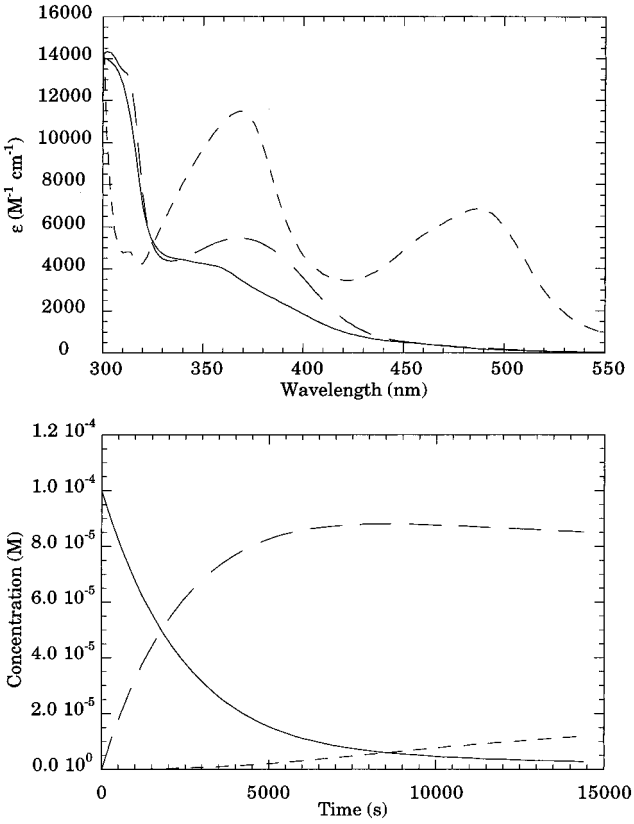

Figure 5. Predicted spectra from the global model for the oxidation of *sec*-phenylethanol described in the text for complexes of Ru(II)OH_2 (- -), Ru(III)OH (− −) and Ru(IV)O (s*M*) (top) and the predicted concentration profiles (bottom).

$$Ru^{IV}O^{2+} + Ru^{II}OH_2{}^{2+} \underset{k_3}{\overset{k_2}{\rightleftharpoons}} 2Ru^{III}OH^{2+} \qquad (6)$$

where $k_{1,obs}$ is the pseudo first-order rate constant for the oxidation of *sec*-phenylethanol and k_2 and k_3 are the second-order rate constants for comproportionation and disproportionation. The predicted spectra for the three complexes are shown in Figure 5 along with the concentration profiles over the course of the reaction. In the initial stage of the reaction, the reduction of Ru(IV) to Ru(II) is followed by rapid comproportionation of Ru(II) with the excess Ru(IV) to yield Ru(III). The concentration of Ru(III) achieves a maximum value but then falls as these oxidizing equivalents are lost via the disproportionation to Ru(II) and Ru(IV). *Unlike with the tpy complexes, reactions involving direct oxidation of substrate by the Ru(III) form were not required in the model to fit the data,* which greatly simplifies the kinetic analysis and requires only a single rate constant that involves substrate oxidation (eq 5).

To verify the pseudo first-order nature of eq 5, the returned values of $k_{1,obs}$ were plotted versus concentration of *sec*-phenylethanol to give a straight line whose slope corresponded to a second-order rate constant of $k_1 = 0.014$ M^{-1} s^{-1} for eq 7

$$Ru^{IV}O^{2+} + PhCH(OH)CH_3 \xrightarrow{k_1} Ru^{II}OH_2{}^{2+} + PhCOCH_3 \qquad (7)$$

(plot given in the Supporting Information). The activation parameters determined from an Eyring plot for *sec*-phenylethanol are $\Delta H^{\ddagger} = 7$ kcal mol^{-1} and $\Delta S^{\ddagger} = -70$ cal deg^{-1} mol^{-1} (plot given in the Supporting Information). The values returned for k_2 and k_3 were uncorrelated with concentration and of similar magnitude ($\sim 10^4$ M^{-1} s^{-1}) to those reported for the corresponding comproportionation reactions for other Ru(tpy)(bpy)O^{2+} derivatives,[36] and the ratio k_2/k_3 remained constant at

(35) Thompson, M. S.; Meyer, T. J. *J. Am. Chem. Soc.* **1982**, *104*, 5070.
(36) Thompson, M. S.; Meyer, T. J. *J. Am. Chem. Soc.* **1982**, *104*, 4106.
(37) Johnston, D. H.; Glasgow, K. C.; Thorp, H. H. *J. Am. Chem. Soc.* **1995**, *117*, 8933−8938.

Table 3. Rate Constants and Activation Parameters for Oxidations of *sec*-Phenylethanol and *trans*-Stilbene

complex	substrate	k (M^{-1} s^{-1})	$\Delta H^{\ddagger}$ (kcal mol^{-1})	$\Delta S^{\ddagger}$ (cal deg^{-1} mol^{-1})
$[(DAMP)(bpy)RuO]^{2+}$	phenylethanol	0.014	7	−70
$[(bpy)_2(py)RuO]^{2+}$	phenylethanol	2.63	5.7	−38
$[(DAMP)(bpy)RuO]^{2+}$	*trans*-stilbene	0.0014	8	−70
$[(bpy)_2(py)RuO]^{2+}$	*trans*-stilbene	0.280	4.4	−46

230 ± 10, which agrees with the value predicted by the Nernst equation for comproportionation of two redox couples separated by 140 mV. The values for $k_{1,obs}$, k_2, and k_3 as a function of substrate concentration are given in the Supporting Information.

We have discussed in detail elsewhere the mechanisms of nonproductive self-inactivation of oxoruthenium(IV) complexes.[16] This reaction has particularly profound implications in DNA reactions, where local concentrations are increased by binding of the cationic complexes to the polyanion. We have discussed these implications as a model for the self-inactivation of activated iron bleomycin.[38] The plot of $k_{1,obs}$ versus the *sec*-phenylethanol concentration exhibited a nonzero intercept at 4.8×10^{-5} s^{-1}, which represents the first-order rate constant for self-inactivation of the oxoruthenium(IV) form:

$$Ru^{IV}O^{2+} \xrightarrow{k_x} Ru^{II}OH^{2+} \qquad (8)$$

As expected, the self-inactivation rate constant (k_x) was independent of metal concentration, and the disappearance of $Ru^{IV}O^{2+}$ in the absence of substrate was a single-exponential, consistent with a first-order rate constant for k_x. In the reactions with *sec*-phenylethanol and *trans*-stilbene, the substrate concentration under pseudo-first-order conditions was kept large enough so that k_x could be neglected in determining the second-order rate constants for substrate oxidation.

The oxidation of *sec*-phenylethanol by oxometal complexes is believed to occur through hydride abstraction to yield acetophenone.[33] For 5 mM $[(DAMP)(bpy)RuO]^{2+}$, a $91 \pm 5\%$ yield of acetophenone was observed when a large excess (100 mM) of substrate was present, indicating that the complex is an effective two-electron oxidant. At lower substrate concentrations, however, much lower (20−40%) yields were obtained due to competition from self-inactivation (eq 5). A table of yields of acetophenone obtained at different substrate:metal ratios is given in the Supporting Information.

Similar spectral changes were observed during the oxidation of *trans*-stilbene by $[(DAMP)(bpy)RuO]^{2+}$ in acetonitrile (spectra given in the Supporting Information). The changes are characterized by the growth of MLCT absorptions of $[(DAMP)(bpy)RuNCMe]^{2+}$ centered at 352 and 454 nm. These gross features are similar to the observations with $[(bpy)_2(py)RuO]^{2+}$;[28] however, no evidence for any substrate-bound complex intermediates was obtained in the case of the less oxidizing DAMP complex. Singular value decompostition of the time-dependent spectra confirmed the presence of only two significant sets of eigenvectors consistent with a simple pseudo-first-order A → B mechanism:

$$Ru^{IV}O^{2+} \xrightarrow{k_{4,obs}} Ru^{II}OH_2{}^{2+} \qquad (9)$$

The second-order rate constant obtained from a plot of $k_{4,obs}$ versus [*trans*-stilbene] is $k_4 = 0.0014$ M^{-1} s^{-1}, and the activation parameters $\Delta H^{\ddagger}$ and $\Delta S^{\ddagger}$ are 8 kcal mol^{-1} and −70 cal deg^{-1} mol^{-1}, respectively (plots given in the Supporting Information). *trans*-Stilbene oxide was detected by GC-MS, but the high substrate:metal ratios required prohibited accurate quantitation.

(38) Worth, L., Jr.; Frank, B. L.; Christner, D. F.; Absalon, M. J.; Stubbe, J.; Kozarich, J. W. *Biochemistry* **1993**, *32*, 2601.

Table 4. Representative Rate Constants during Oxidation of Nucleic Acids by 100 μM $[(DAMP)(L)RuO]^{2+}$ Where L = bpy, phen, and dppz

L	nucleic acid	[nucleic acid] (mM)	$10^5 k_{5,obs}$ (s^{-1})
bpy	none	0	4.8 ± 0.2
	CT-DNA	1.0	7.6 ± 0.2
		1.5	7.7 ± 0.2
		2.0	9.7 ± 0.2
		2.5	10.0 ± 0.2
		3.0	11.0 ± 0.2
	5′-dCMP	50	6.9 ± 0.2
	5′-dTMP	50	6.2 ± 0.2
	5′-dAMP	50	11.1 ± 0.2
phen	CT-DNA	1.0	18.0 ± 0.2
dppz		1.0	2.1 ± 0.2

The rate constants and activation parameters for the oxidations described above are listed in Table 3 along with similar parameters for $[(bpy)_2(py)RuO]^{2+}$.

Oxidation of Nucleic Acids by $[(DAMP)(L)RuO]^{2+}$ Complexes. Oxidations of polymeric and monomeric nucleic acids were monitored via changes in the visible absorption spectra during the initial phase of the reaction in which the concentration of $Ru^{II}OH_2{}^{2+}$ is negligible. The spectral kinetics data were subjected to singular value decomposition and fit to the first-order A → B case:

$$Ru^{IV}O^{2+} \xrightarrow{k_{5,obs}} Ru^{II}OH^{2+} \qquad (10)$$

The measured rates therefore monitor the conversion of $Ru^{IV}O^{2+}$ to $Ru^{III}OH^{2+}$ regardless of whether this conversion occurs via direct hydrogen atom transfer or via hydride transfer followed by rapid comproportionation (i.e. eqs 5 and 6). The values of $k_{5,obs}$ in various nucleic acid solutions are presented in Table 4.

Inspection of the values of $k_{5,obs}$ for reduction of $[(DAMP)(bpy)RuO]^{2+}$ in calf thymus DNA solution reveal only a slight enhancement beyond the self-inactivation rate constant. However, consideration of only the rate enhancement ($k_{5,obs} - k_x$) as a function of DNA concentration reveals a saturation response reminiscent of the binding isotherm for weakly binding complexes (see the Supporting Information).[19,20,31] There is no evidence of a pre-steady-state "burst fraction" upon mixing that would indicate immediate reduction of complexes upon binding as observed in the tpy family of oxidants.[15] The ratios of $k_{5,obs}$ in the absence and presence of DNA predict that at least half the available oxidizing equivalents are lost to self-inactivation (eq 5). The kinetics of reduction of $[(DAMP)(bpy)RuO]^{2+}$ were also examined in the presence of the nucleotides 5′-dTMP, 5′-dCMP, and 5′-dAMP, which can only undergo sugar oxidation chemistry. Even at very high nucleotide concentrations, the enhancement in $k_{5,obs}$ is at most equivalent to the self-inactivation rate constant k_x.

The oxidation of 5′-dGMP by $[(DAMP)(bpy)RuO]^{2+}$ does proceed with a pseudo-first-order rate constant that is strongly dependent on nucleotide concentration. The plot of $k_{5,obs}$ vs [5′-dGMP] in Figure 6 reveals a curved response consistent with a rapid preequilibrium due to binding of the dicationic complex with the dianionic nucleotide:

$$Ru^{IV}O^{2+} + 5'\text{-dGMP} \overset{K_{eq}}{\rightleftharpoons} Ru^{IV}O^{2+}\cdot 5'\text{-dGMP} \qquad (11)$$

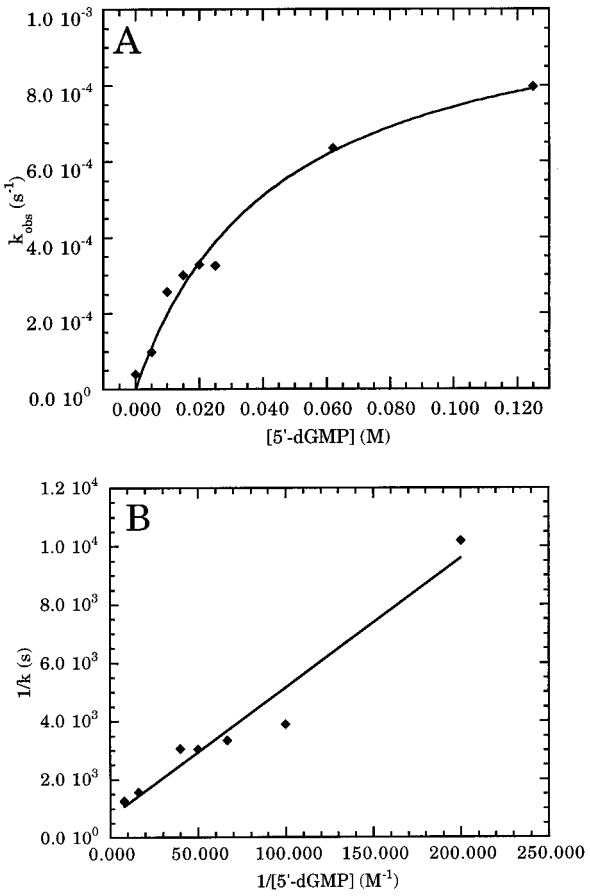

Figure 6. Plot of $k_{5,obs}$ vs [5′-dGMP] (top) and inverse−inverse plot for oxidation of 5′-dGMP by 100 μM [(DAMP)(bpy)RuO]$^{2+}$ in 50 mM phosphate buffer (bottom).

$$Ru^{IV}O^{2+}\cdot 5'\text{-dGMP} \xrightarrow{k_{GMP}} Ru^{II}OH_2{}^{2+} + 5'\text{-dGMP}_{ox} \quad (12)$$

Also presented in Figure 6 is an inverse-inverse plot of $1/k_{5,obs}$ versus 1/[5′-dGMP]. A value for k_{GMP} of 0.0014 s^{-1} can be determined from the reciprocal of the *y*-intercept, and a K_{eq} for eq 11 of 16 M^{-1} can be determined from the *x*-intercept. Similar values of K_{eq} have been measured for analogous reactions of [(tpy)(bpy)RuO]$^{2+}$ with mononucleotides.[14] The product $K_{eq}k_{GMP}$ yields a second-order rate constant of $k_5 = 0.022$ M^{-1} s^{-1} for oxidation of 5′-dGMP by [(DAMP)(bpy)RuO]$^{2+}$. The analogous oxidation of 5′-dGMP by [(tpy)(bpy)RuO]$^{2+}$ proceeds with an estimated second-order rate constant of 9 M^{-1} s^{-1} to yield a putative 8-oxoguanosine monophosphate that is itself more easily oxidized than 5′-dGMP.[14] Unlike oxidations with [(tpy)(bpy)RuO]$^{2+}$, oxidations with [(DAMP)(bpy)RuO]$^{2+}$ fail to yield any products with UV spectra similar to 8-oxoguanine, nor is there any kinetic evidence for overoxidation of any products.

Hairpin Oligonucleotide Oxidation. In the case of [(tpy)(bpy)RuO]$^{2+}$, the oxidant is competent in hydride abstractions at 1′ sugar carbons and oxidations of guanine via an oxygen atom transfer mechanism.[14,16] Oxidation at the 1′ position results in base release to yield a 2′-deoxyribonolactone that provides a combination of frank and base-labile strand scission while guanosine is thought to be oxidized initially to 8-oxoguanosine, which is itself easily oxidized by oxoruthenium. Neither of these lesions is stable in base, and treatment with piperidine therefore results in strand cleavage to yield unmodified 3′ and 5′ phosphate termini to mark the locus of the damaged nucleoside. The fundamental chemical reactions are analogous to many reported for oxidations of alcohols, olefins, and aromatics by oxoruthenium, although the kinetics of oxoruthenium reduction in nucleic acid solution overwhelmingly reflect self-inactivation.[14,16,28,35,36]

Scheme 2

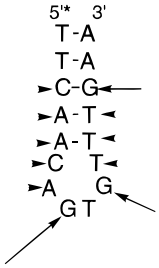

Just as the different nucleotides exhibit different reactivities with a given oxidant, reactivity of polymeric nucleic acids varies widely based on base composition and secondary structure.[14,16,39,40] It has been demonstrated that [(tpy)(bpy)RuO]$^{2+}$ cleaves the mRNA from the iron recognition element (IRE) at only a single G in a hairpin loop in an 80-nucleotide fragment but cleaves the 16-nucleotide DNA analogue of the loop (d[5′-TTCAACAGTGTTTGAA]) at nearly every site.[14,41,42] The cleavage efficiencies vary widely at each site on the hairpin, which has therefore been chosen as a basis to compare the reactivities of the different oxoruthenium complexes. The cleavage pattern for [(DAMP)(bpy)RuO]$^{2+}$ is very similar to that for [(tpy)(bpy)RuO]$^{2+}$, although a 20-fold larger concentration of the DAMP complex resulted in only 10% of the cleavage observed with the tpy analogue (Scheme 2; cleavage intensities given in the Supporting Information). Frank, nonspecific cleavage is observed with a significant piperidine enhancement, which is consistent with sugar oxidation at the 1′ position.[16,43] The enhanced cleavage at G residues is realized only after piperidine treatment, which is consistent with base oxidation as observed in numerous systems.[16,44] The cleavage chemistry of the DAMP and tpy complexes differ only in the relative rates and not in the intimate mechanism or reaction products.

The larger concentrations required are consistent with the lower reactivity of the DAMP complex. Importantly, significant cleavage of the hairpin by the DAMP complex was observed at A and T sites, where the oxidation mechanism involves hydrogen abstraction,[14,16] even though reduction of [(DAMP)(bpy)RuO]$^{2+}$ by 5′-TMP and 5′-AMP was not competitive with self-inactivation. This result implies that sugar oxidation in the hairpin is a result of catalysis of the C−H bond activation by the oligomeric DNA.

Oxidation of DNA by [(DAMP)(bpy)RuOH]$^{2+}$. The kinetics of reduction of [(DAMP)(bpy)RuOH]$^{2+}$ in aqueous DNA solution were studied after visible absorption spectroscopy revealed that *incubation of this complex in the presence of DNA led to quantitative recovery of the* $Ru^{II}OH_2{}^{2+}$ *complex even though the* $Ru^{III}OH^{2+}$ *complex is kinetically stable in buffer.* Changes in the visible absorption of 100 μM [(DAMP)(bpy)RuOH]$^{2+}$ in the presence of 1.0 mM calf thymus DNA are presented in Figure 7. The changes are characterized by return of the MLCT bands *at a rate that is unchanged over at least three quarters of the lifetime of the reaction.* This disappearance

(39) Tullius, T. D.; Dombroski, B. A. *Science (Washington, D.C.)* **1985**, *230*, 679.
(40) Burkhoff, A. M.; Tullius, T. D. *Nature (London)* **1988**, *331*, 455.
(41) Thorp, H. H.; McKenzie, R. A.; Lin, P.-N.; Walden, W. E.; Theil, E. C. *Inorg. Chem.* **1996**, *35*, 2773−2779.
(42) Carter, P. J.; Cheng, C.-C.; Thorp, H. H. *Inorg. Chem.* **1996**, *35*, 3348−3354.
(43) Goyne, T. E.; Sigman, D. S. *J. Am. Chem. Soc.* **1987**, *109*, 2846.
(44) Burrows, C. J.; Rokita, S. E. *Acc. Chem. Res.* **1994**, *27*, 295−301.

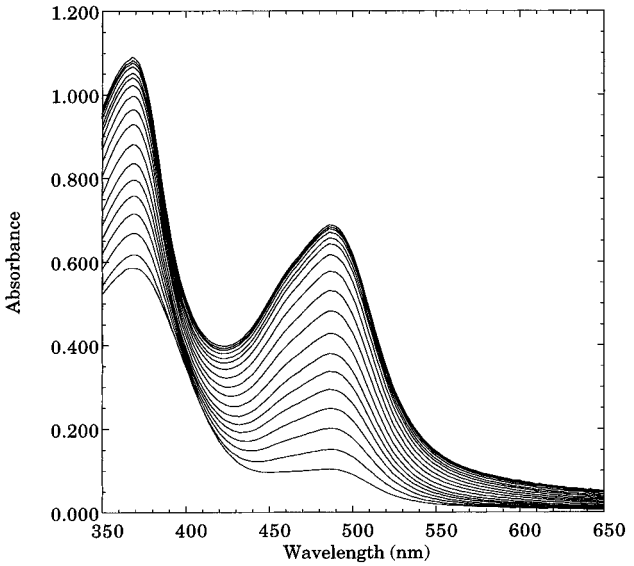

Figure 7. UV−visible spectral changes at 3 h intervals during the reaction of 100 μM [(DAMP)(bpy)RuOH]$^{2+}$ with 1.0 mM calf-thymus DNA in 50 mM phosphate buffer at pH 7.

of [(DAMP)(bpy)RuOH]$^{2+}$ with a zero-order rate law suggests a mechanism involving a catalyst under substrate-saturation conditions.

The spectral kinetics data were subjected to singular value decomposition using the SPECFIT program to yield two significant sets of spectral and evolutionary eigenvectors. These data were fit to a zero-order model:

$$Ru^{III}OH^{2+} \xrightarrow{k_6} Ru^{II}OH_2{}^{2+} \tag{13}$$

$$-d[Ru^{III}OH^{2+}]/dt = k_6 \tag{14}$$

The global analysis of the raw data shown in Figure 7 returned the predicted spectra shown in Figure 8 (top) and a reaction rate of 5.1×10^{-10} M s^{-1}. The bottom panel of Figure 8 shows a plot of absorbance at 486 nm versus time with the predicted values overlaid and confirms good time-based adherence to the zero-order model. Because eq 13 involves the interconversion of only two species, the absorbance versus time traces appear identical for all wavelengths except for the magnitude of the change in absorbance.

To determine whether DNA plays a catalytic role, the concentration dependences of both nucleic acid and metal complex on the reaction rate were determined. The rate (k_6) as a function of added DNA (Figure 9, top) in the presence of 100 μM [(DAMP)(bpy)RuOH]$^{2+}$ exhibits the curved response as function of added nucleotide phosphate typical of a rapid preequilibrium involving DNA binding. Because classical enzyme kinetics states that rate should be directly proportional to enzyme concentration,[45] we hypothesized that the territory occupied by the metal complex on the DNA strand must correspond to the enzyme in this model. The enzyme concentration must remain constant during the reaction, which will occur as long as the DNA is in pseudo-first-order excess. Further, while the DNA territories in heterogeneous calf thymus DNA are not all identical, the sequence variations in the binding mode are too small to affect the kinetic analysis, especially for complexes that bind only electrostatically; this point is supported by other reactions we have reported.[15,16] The effective enzyme

(45) Stryer, L. *Biochemistry*; 3rd ed.; W. H. Freeman and Co.: New York, 1988.

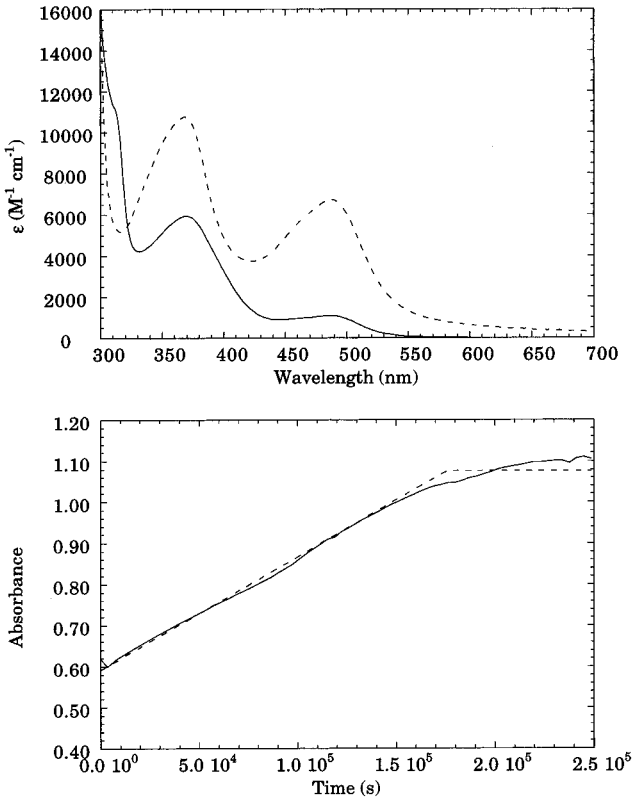

Figure 8. Predicted spectra from analysis of the raw data in Figure 7 for the reduction of [(DAMP)(bpy)RuOH]$^{2+}$ by calf thymus DNA for [(DAMP)(bpy)RuOH]$^{2+}$ and [(DAMP)(bpy)RuOH$_2$]$^{2+}$ from the fit to the zero-order model (top) and absorbance at 486 nm vs time (bottom).

concentration is therefore the concentration of territories available for binding, which is the same as the concentration of total bound metal complex in any oxidation state. We have measured independently the binding constant for [(DAMP)(bpy)RuOH$_2$]$^{2+}$ (Table 2), and we can assume that the binding constants of the Ru^{IV}O^{2+}, Ru^{III}OH^{2+}, and Ru^{II}OH$_2{}^{2+}$ forms are the same since all three forms have the same charge.[26] Previous kinetic studies support this assumption.[15] We can therefore use the measured K_b for the Ru(II) form to estimate the mole fraction of total bound ruthenium (X_b), which is the same as the concentration of available binding territories:

$$X_b = K_b[DNA]/(K_b[DNA] + 1) \tag{15}$$

The plot of reaction rate versus X_b calculated from eq 14 for $K_b = 920$ M^{-1} is linear as shown in Figure 9 (top).

The linear dependence of the reaction rate on the amount of bound metal complex suggested a rapid preequilibrium involving binding of the metal complex to DNA, and the metal-complex concentration dependence was found (via a double-reciprocal plot) to support the rate law (Figure 9, bottom):

$$\text{rate} = kX_b[RuOH^{2+}]_0/(K_m + [RuOH^{2+}]_0) \tag{16}$$

The double-reciprocal plot yields a slope equal to $kX_b[RuOH^{2+}]_0/K_m$ and intercept equal to $(kX_b[RuOH^{2+}]_0)^{-1}$. From the plot shown in the lower panel of Figure 9, we measure a slope of 79 100 M^{-2} s and an intercept of 1.69×10^8 M^{-1} s corresponding to values of $kX_b[RuOH^{2+}]_0$ and K_b equal to 5.9×10^{-9} M s^{-1} and 2100 M^{-1}, respectively. The observed maximum rate in the presence of 3.0 mM DNA is 1.3×10^{-9} M s^{-1}, which is in reasonable agreement with the $kX_b[RuOH^{2+}]_0$ value, which is calculated as an inverse. Further, the binding constant (K_b) obtained from the double-reciprocal plot is in reasonable

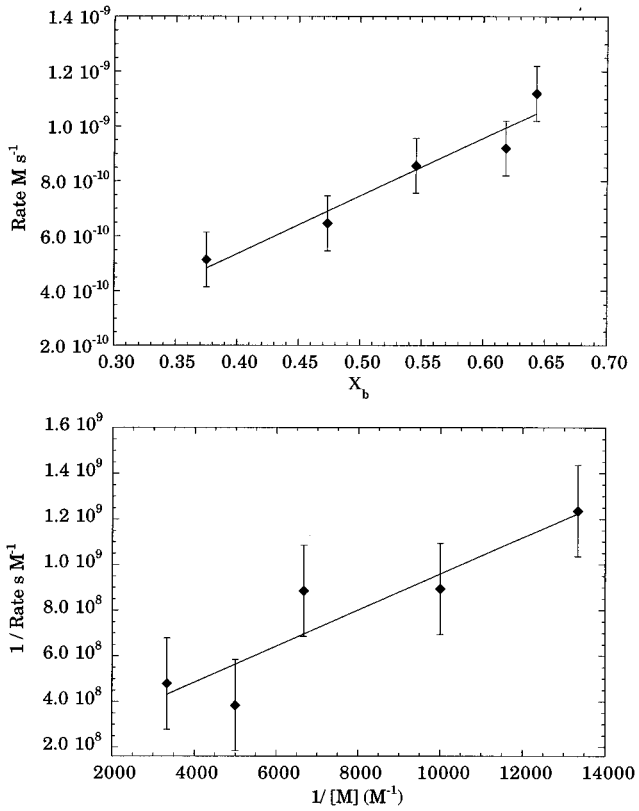

Figure 9. Top: Dependence of k_6 on DNA concentration at 100 μM [(DAMP)(bpy)RuO]$^{2+}$ plotted as a function of X_b calculated from eq 15 and the measured DNA binding constant for [(DAMP)(bpy)RuO]$^{2+}$. Bottom: Dependence of k_6 on [(DAMP)(bpy)RuO]$^{2+}$ concentration at 1.0 mM DNA plotted as a double-reciprocal plot. All rate constants measured in 50 mM phosphate buffer, pH 7. Error bars are determined from standard deviations of the individual rate constants.

agreement with that of 920 M^{-1} shown in Table 2. Finally, the value of $kX_b[RuOH^{2+}]_0$ implies a value of $k = 1.3 \times 10^{-5}$ s^{-1}, which compares favorably with the first-order rate constant for self-inactivation of [(DAMP)(bpy)RuO]$^{2+}$. Because of this similarity, we conclude that the DNA strand catalyzes the unfavorable disproportionation of $Ru^{III}OH^{2+}$ to $Ru^{IV}O^{2+}$ and $Ru^{II}OH_2{}^{2+}$ (eq 1). The $Ru^{IV}O^{2+}$ complex then loses the two oxidizing equivalents in a rate-limiting step through either self- or DNA oxidation with a first-order rate constant of $\sim 10^{-5}$ s^{-1}. The total mechanism consistent with the kinetic observations is as follows:

$$Ru^{III}OH^{2+} + DNA \rightleftharpoons Ru^{III}OH^{2+}\cdot DNA \qquad (17)$$

$$2Ru^{III}OH^{2+}\cdot DNA \rightleftharpoons Ru^{IV}O^{2+}\cdot DNA + Ru^{II}OH_2{}^{2+}\cdot DNA \qquad (18)$$

$$Ru^{IV}O^{2+}\cdot DNA \rightarrow Ru^{II}OH_2{}^{2+}\cdot DNA \qquad (19)$$

Here eq 19 is rate-limiting.

Discussion

Redox Mechanisms. There are two important conclusions from the electronic properties and small molecule oxidations that relate to the DNA kinetics. The first is that reactions involving the direct oxidation of substrate by $Ru^{III}OH^{2+}$ are not required to fit the kinetics data. This point is strikingly apparent in the *sec*-phenylethanol case, where the only reactions considered are two-electron oxidation of substrate by $Ru^{IV}O^{2+}$ and the disproportionation reaction. Considerably more complex models are needed for the more oxidizing tpy complex where $Ru^{III}OH^{2+}$ can directly oxidize substrate.[14,28] The reason that the $Ru^{III}OH^{2+}$ reactivity has been shut off is apparent in the structural and electronic properties. The electrochemical data show that the Ru(III) state is stabilized by 0.15 V relative to the tpy analog, and the crystal structures show clear protection of the reactive oxygen functionalilty by the methyl groups of the damp ligand. So the high-valent forms of the complex are stabilized both kinetically and thermodynamically.

The second important point is that the available mechanistic pathways for the $Ru^{IV}O^{2+}$ oxidant were not changed by substitution of DAMP for tpy. The second-order rate constants fall in the order GMP > *sec*-phenylethanol > *trans*-stilbene for both the tpy case or the DAMP complex. Stabilization of the $Ru^{III}OH^{2+}$ form naturally results in similar stabilization of the $Ru^{IV}O^{2+}$ state; however, the trends in reactivity for the oxo complex were not altered.

DNA Catalysis. The oxidation kinetics and relative yields of cleavage at sites on the DNA strand can now be rationalized in terms of binding affinity and reactivity. Comparision of the kinetics of reduction of [(tpy)(bpy)RuO]$^{2+}$ and [(DAMP)(bpy)-RuO]$^{2+}$ upon mixing with DNA reveal the importance of the relative values of the rate constants for binding, dissociation, DNA oxidation, and self-inactivation. Neyhart et al. showed that, upon mixing solutions of [(tpy)(L)RuO]$^{2+}$ with DNA, a significant fraction proportional to the binding affinity governed by L was immediately reduced.[15] These studies relied on absorbance changes at the isosbestic point for the $Ru^{III}OH^{2+}$ and $Ru^{II}OH_2{}^{2+}$ complexes, but presumably this "burst fraction" represents the establishment of equilibrium concentrations of $Ru^{IV}O^{2+}$, $Ru^{III}OH^{2+}$, and $Ru^{II}OH_2{}^{2+}$ *in the vicinity of the DNA strand* according to k_2 and k_3 (eqs 5 and 6). The remaining $Ru^{IV}O^{2+}$ in solution must be reduced after exchange with a bound complex, and this rate constant therefore does not depend on DNA or metal complex concentration. No burst fraction is observed upon mixing [(DAMP)(bpy)RuO]$^{2+}$ with DNA, thereby showing that high local concentrations of $Ru^{IV}O^{2+}$ can be maintained in the vicinity of the DNA strand. The value of $k_{5,obs} - k_x$, the pseudo-first-order rate constant for DNA oxidation, therefore follows an isotherm dependence on DNA concentration consistent with a rate proportional to X_b (plot given in the Supporting Information).

Oxidation of free TMP by [(DAMP)(bpy)RuO]$^{2+}$ was not observed, indicating that the complex is not a competent oxidant of free sugar. However, cleavage of the hairpin was clearly observed at A and T sites that must react via sugar oxidation. The oligomeric structure of the hairpin is therefore promoting the sugar oxidation. This effect presumably arises through an increase in the local concentration due to DNA binding. Accordingly, more sugar oxidation is observed in the stem and stem−loop junction regions of the hairpin, where binding of the cationic complex should occur with higher affinity than in the single-stranded loop region.

A number of features of the kinetics of reduction of [(DAMP)(bpy)RuOH]$^{2+}$ are noteworthy. First, zero-order kinetics are observed, consistent with true catalytic behavior. Second, the kinetics can be analyzed using a model analogous to the Michaelis-Menton model, where the territory of DNA that binds the metal complex is analogous to the enzyme. Since calf thymus DNA contains many sequences, the ensemble of territories are all slightly different from a sequence point of view; however, the reactivity of the bound complex does not vary enough to allow reaction in different binding modes or sequences to be differentiated. This behavior is consistent with simple electrostatic binding, as we have discussed in detail

elsewhere.[15−17,19,46] The catalysis is readily apparent in that the $Ru^{III}OH^{2+}$ complex is kinetically stable in buffer; however, quantitative conversion to $Ru^{II}OH_2^{2+}$ is observed in the presence of DNA. This effect likely arises from catalysis of the disproportionation to $Ru^{IV}O^{2+}$ and $Ru^{II}OH_2^{2+}$ by enhancement of the local concentration of $[(DAMP)(bpy)RuOH]^{2+}$. According to calculations by Manning,[47] territorial electrostatic binding of an *N*-valent cation displaces two sodium counterions from a volume about the double strand to yield a local concentration given by

$$C_N^{\,loc} = (10^3/V_p)(C_b/[DNA]) \qquad (20)$$

where V_p (646 cm^3 mol^{-1} for double-stranded DNA) is the volume of the region within which the cation is said to be bound, C_b is the bulk concentration of complex bound, and the DNA concentration is the molarity of the nucleotide phosphate. Given a binding constant of 900 M^{-1}, 100 μM $[(DAMP)(bpy)RuOH]^{2+}$ will partition to 47 μM bound and 53 μM free in the presence of 1.0 mM DNA. Substitution of the appropriate values for C_b and [DNA] in eq 15 yields a value of C_N^{loc} equal to 73 mM. The local concentration has thus been enhanced by a factor of 1400. This enhancement implies that the rate of disproportionation of bound $[(DAMP)(bpy)RuOH]^{2+}$ will be enhanced by $\sim 2 \times 10^6$. This analysis assumes noncooperative binding of the metal complex to DNA, which is apparent in the electrochemical titrations reported in Table 2. The cooperative binding of intercalating metal complexes to DNA has been a subject of recent intense interest;[48,49] however, there is no evidence to support the cooperative binding of nonintercalating complexes such as $[(DAMP)(bpy)RuOH]^{2+}$. Cooperative binding would lead to larger rate enhancements, but since a large enhancement is already possible via eq 20, cooperative binding is not necessary to realize DNA catalysis.

Comparison with Other DNA Catalysis Systems. The studies reported here provide a more quantitative view of DNA catalysis from the point of view of the kinetic model; however, the origin of the catalysis is very similar to that observed in promotion of bimolecular electron-transfer reactions[1,2,50] and covalent labeling of GG sites in oligomers.[8] Namely, the effect arises from an increase in the local concentration of the metal complex due to electrostatic condensation. In the present case, we have shown that the enzyme−substrate complex is analogous to the $Ru^{III}OH^{2+}$·DNA adduct, which is the species that decomposes in the rate-limiting step. Accordingly, the overall reaction proceeds with zero-order kinetics and can be analyzed according to an enzyme model (Figures 8 and 9). Determination of the appropriate first-order rate constant from the fitted model is in good agreement with the measured rate constant for self-inactivation and DNA oxidation by $[(DAMP)(bpy)RuO]^{2+}$, and the model yields a binding constant in good agreement with that from independent measurement. This information provides a firm quantitative basis for the concept of DNA catalysis by electrostatic condensation; however, true enzymatic catalysis would involve not only favorable orientation of the reactants but also stabilization of the transition state.[13] Evidence for transition-state stabilization is not available in this case and remains an attractive target in developing DNA catalysis.

Acknowledgment. This research was supported by the National Science Foundation. T.W.W. thanks the Department of Education for a Graduate Fellowship, and H.H.T. thanks the Camille and Henry Dreyfus Foundation for a Camille Dreyfus Teacher-Scholar Award and the Alfred P. Sloan Foundation for a Fellowship.

Supporting Information Available: Text describing experimental procedures for the preparation of DAMP complexes and the hairpin cleavage reaction, tables of optical spectroscopy data, crystal data and fractional coordinates for $[(DAMP)(bpy)RuO](ClO_4)_2$ and $[(DAMP)(phen)RuO](ClO_4)_2$, yields of acetophenone from oxidation of phenylethanol by $[(DAMP)(bpy)RuO]^{2+}$, and rate constants for eqs 5 and 6 for oxidation of phenylethanol, a cyclic voltammogram of $[(DAMP)(dppz)RuO]^{2+}$, first-order and Eyring plots for oxidation of phenylethanol and *trans*-stilbene by $[(DAMP)(bpy)RuO]^{2+}$, spectral changes for *trans*-stilbene oxidation, a plot of $k_{5,obs} - k_x$ versus [DNA] for oxidation by $[(DAMP)(bpy)RuO]^{2+}$, and a histogram of cleavage intensities used to obtain Scheme 2 (16 pages). Ordering information is given on any current masthead page.

IC9703944

(46) Kalsbeck, W. A.; Thorp, H. H. *Inorg. Chem.* **1994**, *33*, 3427−3429.
(47) Manning, G. S. *Acc. Chem. Res.* **1979**, *12*, 443.
(48) Olson, E. J. C.; Hu, D.; Hörmann, A.; Barbara, P. F. *J. Phys. Chem. B* **1997**, *101*, 299−303.
(49) Lincoln, P.; Tuite, E.; Nordén, B. *J. Am. Chem. Soc.* **1997**, *119*, 1454−1455.
(50) Purugganan, M. D.; Kumar, C. V.; Turro, N. J.; Barton, J. K. *Science* **1988**, *241*, 1645−1649.